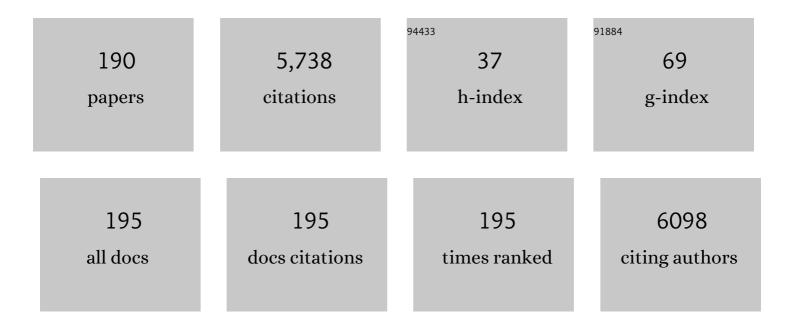
List of Publications by Year in descending order

Source: https://exaly.com/author-pdf/11481293/publications.pdf Version: 2024-02-01



#	Article	IF	CITATIONS
1	Hydrogen storage in Pd nanocrystals covered with a metal–organic framework. Nature Materials, 2014, 13, 802-806.	27.5	412
2	Discovery of Face-Centered-Cubic Ruthenium Nanoparticles: Facile Size-Controlled Synthesis Using the Chemical Reduction Method. Journal of the American Chemical Society, 2013, 135, 5493-5496.	13.7	290
3	Solid Solution Alloy Nanoparticles of Immiscible Pd and Ru Elements Neighboring on Rh: Changeover of the Thermodynamic Behavior for Hydrogen Storage and Enhanced CO-Oxidizing Ability. Journal of the American Chemical Society, 2014, 136, 1864-1871.	13.7	229
4	Platinum-Group-Metal High-Entropy-Alloy Nanoparticles. Journal of the American Chemical Society, 2020, 142, 13833-13838.	13.7	223
5	Strong Phonon–Phonon Interactions Securing Extraordinary Thermoelectric Ge _{1–<i>x</i>} Sb _{<i>x</i>} Te with Zn-Alloying-Induced Band Alignment. Journal of the American Chemical Society, 2019, 141, 1742-1748.	13.7	199
6	Photocatalytic uphill conversion of natural gas beyond the limitation of thermal reaction systems. Nature Catalysis, 2020, 3, 148-153.	34.4	194
7	Arrays of Planar Vacancies in Superior Thermoelectric Ge _{1â^'} <i>_x</i> _{â^'} <i>_y</i> Cd <i>_x</i> Bi <i>_{ with Band Convergence. Advanced Energy Materials, 2018, 8, 1801837.}</i>	y ∢/sus b><,	/i> 1@1
8	A low-crystalline ruthenium nano-layer supported on praseodymium oxide as an active catalyst for ammonia synthesis. Chemical Science, 2017, 8, 674-679.	7.4	149
9	Achieving <i>zT</i> > 2 in pâ€Type AgSbTe _{2â^'} <i>_x</i> Se <i>_x</i> Alloys via Exploring the Extra Light Valence Band and Introducing Dense Stacking Faults. Advanced Energy Materials, 2018, 8, 1702333.	19.5	143
10	Efficient ammonia synthesis over a Ru/La _{0.5} Ce _{0.5} O _{1.75} catalyst pre-reduced at high temperature. Chemical Science, 2018, 9, 2230-2237.	7.4	142
11	On the electronic structure and hydrogen evolution reaction activity of platinum group metal-based high-entropy-alloy nanoparticles. Chemical Science, 2020, 11, 12731-12736.	7.4	142
12	Mechanisms of radiation-induced segregation in CrFeCoNi-based single-phase concentrated solid solution alloys. Acta Materialia, 2017, 126, 182-193.	7.9	133
13	Efficient overall water splitting in acid with anisotropic metal nanosheets. Nature Communications, 2021, 12, 1145.	12.8	124
14	Shape-Dependent Hydrogen-Storage Properties in Pd Nanocrystals: Which Does Hydrogen Prefer, Octahedron (111) or Cube (100)?. Journal of the American Chemical Society, 2014, 136, 10222-10225.	13.7	104
15	Significant Enhancement of Hydrogen Evolution Reaction Activity by Negatively Charged Pt through Light Doping of W. Journal of the American Chemical Society, 2020, 142, 17250-17254.	13.7	103
16	Solid-Solution Alloying of Immiscible Ru and Cu with Enhanced CO Oxidation Activity. Journal of the American Chemical Society, 2017, 139, 4643-4646.	13.7	94
17	Noble-Metal High-Entropy-Alloy Nanoparticles: Atomic-Level Insight into the Electronic Structure. Journal of the American Chemical Society, 2022, 144, 3365-3369.	13.7	94
18	Selective control of fcc and hcp crystal structures in Au–Ru solid-solution alloy nanoparticles. Nature Communications, 2018, 9, 510.	12.8	90

#	Article	IF	CITATIONS
19	Solidâ€Solution Alloy Nanoparticles of the Immiscible Iridium–Copper System with a Wide Composition Range for Enhanced Electrocatalytic Applications. Angewandte Chemie - International Edition, 2018, 57, 4505-4509.	13.8	86
20	Charge transfer dependence on CO ₂ hydrogenation activity to methanol in Cu nanoparticles covered with metal–organic framework systems. Chemical Science, 2019, 10, 3289-3294.	7.4	77
21	Evidence of the hydrogen release mechanism in bulk MgH2. Scientific Reports, 2015, 5, 8450.	3.3	66
22	Enhanced damage resistance and novel defect structure of CrFeCoNi under in situ electron irradiation. Scripta Materialia, 2016, 125, 5-9.	5.2	62
23	Continuous-Flow Reactor Synthesis for Homogeneous 1 nm-Sized Extremely Small High-Entropy Alloy Nanoparticles. Journal of the American Chemical Society, 2022, 144, 11525-11529.	13.7	60
24	Nanosize-Induced Drastic Drop in Equilibrium Hydrogen Pressure for Hydride Formation and Structural Stabilization in Pd–Rh Solid-Solution Alloys. Journal of the American Chemical Society, 2012, 134, 12390-12393.	13.7	59
25	Detection of photons emitted from single erbium atoms in energy-dispersive X-ray spectroscopy. Nature Photonics, 2012, 6, 545-548.	31.4	57
26	Ru/La _{0.5} Pr _{0.5} O _{1.75} Catalyst for Low-Temperature Ammonia Synthesis. ACS Sustainable Chemistry and Engineering, 2018, 6, 17258-17266.	6.7	57
27	In-situ investigation of the hydrogen release mechanism in bulk Mg2NiH4. Journal of Power Sources, 2017, 341, 130-138.	7.8	55
28	Encapsulation of Bimetallic Nanoparticles into a Metal–Organic Framework: Preparation and Microstructure Characterization of Pd/Au@ZIFâ€8. European Journal of Inorganic Chemistry, 2014, 2014, 5514-5521.	2.0	52
29	Nano-scale dislocations induced by self-vacancy engineering yielding extraordinary n-type thermoelectric Pb0.96-yInySe. Nano Energy, 2018, 50, 785-793.	16.0	51
30	Emergence of high ORR activity through controlling local density-of-states by alloying immiscible Au and Ir. Chemical Science, 2019, 10, 652-656.	7.4	50
31	Surface Dynamics for Creating Highly Active Ru Sites for Ammonia Synthesis: Accumulation of a Low-Crystalline, Oxygen-Deficient Nanofraction. ACS Sustainable Chemistry and Engineering, 2020, 8, 2726-2734.	6.7	50
32	Short range order and its transformation to long range order in Ni4Mo. Acta Materialia, 1998, 46, 881-892.	7.9	48
33	Cation disordering in magnesium aluminate spinel crystals induced by electron or ion irradiation. Journal of Nuclear Materials, 2000, 283-287, 952-956.	2.7	48
34	Solid-solution alloy nanoparticles of a combination of immiscible Au and Ru with a large gap of reduction potential and their enhanced oxygen evolution reaction performance. Chemical Science, 2019, 10, 5133-5137.	7.4	48
35	A CO Adsorption Site Change Induced by Copper Substitution in a Ruthenium Catalyst for Enhanced CO Oxidation Activity. Angewandte Chemie - International Edition, 2019, 58, 2230-2235.	13.8	48
36	A Synthetic Pseudo-Rh: NOx Reduction Activity and Electronic Structure of Pd–Ru Solid-solution Alloy Nanoparticles. Scientific Reports, 2016, 6, 28265.	3.3	44

#	Article	IF	CITATIONS
37	The local structure in heavily boron-doped diamond and the effect this has on its electrochemical properties. Carbon, 2018, 137, 333-342.	10.3	44
38	Crystal Structure Control of Binary and Ternary Solid-Solution Alloy Nanoparticles with a Face-Centered Cubic or Hexagonal Close-Packed Phase. Journal of the American Chemical Society, 2022, 144, 4224-4232.	13.7	40
39	Characterising the polymorphic phase transformation at a localised point on a Cu6Sn5 grain. Materials Characterization, 2018, 138, 113-119.	4.4	37
40	Double enhancement of hydrogen storage capacity of Pd nanoparticles by 20 at% replacement with Ir; systematic control of hydrogen storage in Pd–M nanoparticles (M = Ir, Pt, Au). Chemical Science, 2018, 9, 5536-5540.	7.4	37
41	CO2-Free Power Generation on an Iron Group Nanoalloy Catalyst via Selective Oxidation of Ethylene Glycol to Oxalic Acid in Alkaline Media. Scientific Reports, 2014, 4, 5620.	3.3	36
42	Discovery of Hexagonal Structured Pd–B Nanocrystals. Angewandte Chemie - International Edition, 2017, 56, 6578-6582.	13.8	34
43	Characterisation of lithium-ion battery anodes fabricated via in-situ Cu6Sn5 growth on a copper current collector. Journal of Power Sources, 2019, 415, 50-61.	7.8	34
44	Dynamical Behavior of Ordering with Phase Separation in Off-Stoichiometric Fe ₃ Si Alloys. Materials Transactions, JIM, 1989, 30, 695-706.	0.9	32
45	Electron Tomography Imaging and Analysis of <i>γ</i> ′ and <i>γ</i> Domains in Niâ€based Superalloys. Advanced Materials, 2008, 20, 1905-1909.	21.0	31
46	Encapsulation of Bimetallic Metal Nanoparticles into Robust Zirconium-Based Metal-Organic Frameworks: Evaluation of the Catalytic Potential for Size-Selective Hydrogenation. Chemistry - A European Journal, 2017, 23, 3583-3594.	3.3	31
47	Dark-field transmission electron microscopy for a tilt series of ordering alloys: toward electron tomography. Microscopy (Oxford, England), 2005, 54, 373-377.	1.5	30
48	Hydrogen storage and stability properties of Pd–Pt solid-solution nanoparticles revealed via atomic and electronic structure. Scientific Reports, 2017, 7, 14606.	3.3	30
49	Properties of CuGa2 Formed Between Liquid Ga and Cu Substrates at Room Temperature. Journal of Electronic Materials, 2020, 49, 128-139.	2.2	29
50	Fabrication of Integrated Copperâ€Based Nanoparticles/Amorphous Metal–Organic Framework by a Facile Sprayâ€Drying Method: Highly Enhanced CO ₂ Hydrogenation Activity for Methanol Synthesis. Angewandte Chemie - International Edition, 2021, 60, 22283-22288.	13.8	29
51	Kinetics of CuPt-type ordered phase formation in III-V semiconductor alloys during (001) epitaxial growth due to step flow. Physical Review B, 1995, 51, 9707-9714.	3.2	28
52	An ordered bcc CuPd nanoalloy synthesised via the thermal decomposition of Pd nanoparticles covered with a metal–organic framework under hydrogen gas. Chemical Communications, 2014, 50, 13750-13753.	4.1	28
53	Influence of the Crystal Structure of Titanium Oxide on the Catalytic Activity of Rh/TiO ₂ in Steam Reforming of Propane at Low Temperature. Chemistry - A European Journal, 2018, 24, 8742-8746.	3.3	28
54	Barium Oxide Encapsulating Cobalt Nanoparticles Supported on Magnesium Oxide: Active Non-Noble Metal Catalysts for Ammonia Synthesis under Mild Reaction Conditions. ACS Catalysis, 2021, 11, 13050-13061.	11.2	28

#	Article	IF	CITATIONS
55	Enhanced magnetization in highly crystalline and atomically mixed bcc Fe–Co nanoalloys prepared by hydrogen reduction of oxide composites. Nanoscale, 2013, 5, 1489.	5.6	27
56	Firstâ€Principles Calculation, Synthesis, and Catalytic Properties of Rhâ€Cu Alloy Nanoparticles. Chemistry - A European Journal, 2017, 23, 57-60.	3.3	26
57	Dual Lewis Acidic/Basic Pd _{0.5} Ru _{0.5} –Poly(<i>N</i> â€vinylâ€2â€pyrrolidone) Alloyed Nanoparticle: Outstanding Catalytic Activity and Selectivity in Suzuki–Miyaura Crossâ€Coupling Reaction. ChemCatChem, 2015, 7, 3887-3894.	3.7	25
58	Transmission electron microscopy of bulk specimens over 10 µm in thickness. Ultramicroscopy, 2016, 162, 10-16.	1.9	25
59	The Electronic State of Hydrogen in the αâ€Phase of the Hydrogenâ€Storage Material PdH(D) _{<i>x</i>} : Does a Chemical Bond Between Palladium and Hydrogen Exist?. Angewandte Chemie - International Edition, 2018, 57, 9823-9827.	13.8	25
60	Ordered Structures and Phase States in Epitaxial Layers of Ill–V Semiconductor Alloys. Japanese Journal of Applied Physics, 1990, 29, 688-695.	1.5	24
61	Atomically mixed Fe-group nanoalloys: catalyst design for the selective electrooxidation of ethylene glycol to oxalic acid. Physical Chemistry Chemical Physics, 2015, 17, 11359-11366.	2.8	23
62	Synthesis of Mo and Ru solid-solution alloy NPs and their hydrogen evolution reaction activity. Chemical Communications, 2020, 56, 14475-14478.	4.1	23
63	Atom locations in a Ni doped Î(Cu,Ni)6Sn5 intermetallic compound. Scripta Materialia, 2019, 158, 1-5.	5.2	22
64	Highly Stable and Active Solidâ€Solutionâ€Alloy Threeâ€Way Catalyst by Utilizing Configurationalâ€Entropy Effect. Advanced Materials, 2021, 33, e2005206.	21.0	22
65	Accumulation of radiation damage and disordering in MgAl ₂ O ₄ under swift heavy ion irradiation. International Journal of Materials Research, 2011, 102, 1082-1088.	0.3	20
66	Crystal-phase control of GaAs–GaAsSb core–shell/axial nanowire heterostructures by a two-step growth method. Journal of Materials Chemistry C, 2018, 6, 6726-6732.	5.5	20
67	Discovery of face-centred cubic Os nanoparticles. Chemical Communications, 2020, 56, 372-374.	4.1	20
68	Electron tomography imaging methods with diffraction contrast for materials research. Microscopy (Oxford, England), 2020, 69, 141-155.	1.5	19
69	Interfacial Reactions between Ga and Cu-10Ni Substrate at Low Temperature. ACS Applied Materials & Interfaces, 2020, 12, 21045-21056.	8.0	19
70	Nonequilibrium Flow-Synthesis of Solid-Solution Alloy Nanoparticles: From Immiscible Binary to High-Entropy Alloys. Journal of Physical Chemistry C, 2021, 125, 458-463.	3.1	18
71	Frenkel pair accumulation induced crystallization of amorphous MgAl2O4. Journal of Nuclear Materials, 2008, 378, 188-192.	2.7	17
72	Atomic-Resolution X-ray Energy-Dispersive Spectroscopy Chemical Mapping of Substitutional Dy Atoms in a High-Coercivity Neodymium Magnet. Japanese Journal of Applied Physics, 2013, 52, 050201.	1.5	17

#	Article	IF	CITATIONS
73	Effect of trace Na additions on the hydrogen absorption kinetics of Mg ₂ Ni. Journal of Materials Research, 2016, 31, 1316-1327.	2.6	17
74	Intermetallic formation mechanisms and properties in room-temperature Ga soldering. Journal of Alloys and Compounds, 2020, 826, 154221.	5.5	17
75	Boosting reverse water-gas shift reaction activity of Pt nanoparticles through light doping of W. Journal of Materials Chemistry A, 2021, 9, 15613-15617.	10.3	17
76	Preparation of solid–solution type Fe–Co nanoalloys by synchronous deposition of Fe and Co using dual arc plasma guns. Dalton Transactions, 2015, 44, 15764-15768.	3.3	16
77	Atomic structure observations and reaction dynamics simulations on triple phase boundaries in solid-oxide fuel cells. Communications Chemistry, 2019, 2, .	4.5	16
78	Highly Correlated Size and Composition of Pt/Au Alloy Nanoparticles via Magnetron Sputtering onto Liquid. Langmuir, 2020, 36, 3004-3015.	3.5	16
79	Facile Synthesis of Size-controlled Rh Nanoparticles via Microwave-assisted Alcohol Reduction and Their Catalysis of CO Oxidation. Chemistry Letters, 2017, 46, 1254-1257.	1.3	16
80	Imaging the Polymorphic Transformation in a Single Cu6Sn5 Grain in a Solder Joint. Materials, 2018, 11, 2229.	2.9	15
81	Preparation and Growth Mechanism of Pt/Cu Alloy Nanoparticles by Sputter Deposition onto a Liquid Polymer. Langmuir, 2019, 35, 8418-8427.	3.5	15
82	Rational Synthesis for a Noble Metal Carbide. Journal of the American Chemical Society, 2020, 142, 1247-1253.	13.7	15
83	Electron microscopic observation and its interpretation of Ostwald ripening in precipitation dynamics in alloys. Phase Transitions, 1987, 8, 213-225.	1.3	14
84	Monte Carlo simulation of CuPtâ€type ordering in offâ€stoichiometric IIIâ€V semiconductor alloys. Journal of Applied Physics, 1995, 77, 2370-2374.	2.5	14
85	Diffuse scattering in partially ordered III-V semiconductor alloys. Physical Review B, 1995, 52, 5154-5159.	3.2	14
86	Evidence of Copper Separation in Lithiated Cu ₆ Sn ₅ Lithium-Ion Battery Anodes. ACS Applied Energy Materials, 2020, 3, 141-145.	5.1	14
87	Microstructure evolution of NiO–YSZ cermet during sintering. Solid State Ionics, 2014, 262, 460-464.	2.7	13
88	Observation of the Ni/YSZ Interface in a Conventional SOFC. Journal of the Electrochemical Society, 2015, 162, F750-F754.	2.9	13
89	Solidâ€Solution Alloy Nanoparticles of the Immiscible Iridium–Copper System with a Wide Composition Range for Enhanced Electrocatalytic Applications. Angewandte Chemie, 2018, 130, 4595-4599.	2.0	13
90	Atomic Insights into Phase Evolution in Ternary Transitionâ€Metal Dichalcogenides Nanostructures. Small, 2018, 14, e1800780.	10.0	13

#	Article	IF	CITATIONS
91	Coreduction methodology for immiscible alloys of CuRu solid-solution nanoparticles with high thermal stability and versatile exhaust purification ability. Chemical Science, 2020, 11, 11413-11418.	7.4	13
92	Precipitation Behavior in a Cu-4.5 wt%Co Alloy. Japanese Journal of Applied Physics, 1981, 20, L605-L608.	1.5	12
93	An Analytical Electron Diffraction Technique for the Determination of Long-Range Order Parameters in Multi-Component Ordered Alloys. Materials Transactions, JIM, 1991, 32, 905-910.	0.9	12
94	Kinetics of irradiation-induced phase transformations in tricritical systems. Physical Review B, 1996, 54, 6184-6193.	3.2	12
95	<i>In situ</i> observation of structural transformation of gold nanorods under pulsed laser irradiation in an HVEM. Microscopy (Oxford, England), 2014, 63, 261-268.	1.5	12
96	Kinetics of the β → α Transformation of Tin: Role of α-Tin Nucleation. Crystal Growth and Design, 2015, 15, 5767-5773.	3.0	12
97	Detection of picometer-order atomic displacements in drift-compensated HAADF-STEM images of gold nanorods. Microscopy (Oxford, England), 2016, 65, 391-399.	1.5	12
98	The effects of Ni on inhibiting the separation of Cu during the lithiation of Cu6Sn5 lithium-ion battery anodes. Journal of Power Sources, 2019, 440, 227085.	7.8	12
99	A CO Adsorption Site Change Induced by Copper Substitution in a Ruthenium Catalyst for Enhanced CO Oxidation Activity. Angewandte Chemie, 2019, 131, 2252-2257.	2.0	11
100	Effect of Calcination and Reduction Temperatures on the Catalytic Activity of Ru/La _{0.5} Ce _{0.5} O _{1.75} for Ammonia Synthesis under Mild Conditions. Energy Technology, 2020, 8, 2000264.	3.8	11
101	Atomic resolution imaging of cation ordering in niobium–tungsten complex oxides. Communications Materials, 2021, 2, .	6.9	11
102	Chemoselective hydrogenation of heteroarenes and arenes by Pd–Ru–PVP under mild conditions. RSC Advances, 2020, 10, 44191-44195.	3.6	11
103	Study of temperature factors in cubic crystals by high-voltage electron diffraction. Journal of Electron Microscopy Technique, 1989, 12, 262-271.	1.1	10
104	Effects of Ni and Cu Antisite Substitution on the Phase Stability of CuGa2 from Liquid Ga/Cu–Ni Interfacial Reaction. ACS Applied Materials & Interfaces, 2019, 11, 32523-32532.	8.0	10
105	Epitaxial GaAs/AlGaAs core–multishell nanowires with enhanced photoluminescence lifetime. Nanoscale, 2019, 11, 6859-6865.	5.6	10
106	PM-16Atomic-Resolution Tomography of Metal Alloy Nanoparticles: The Effects of Reconstruction Parameters. Microscopy (Oxford, England), 2017, 66, i25-i25.	1.5	10
107	Mechanism of Hydrogen Storage and Structural Transformation in Bimetallic Pd–Pt Nanoparticles. ACS Applied Materials & Interfaces, 2021, 13, 23502-23512.	8.0	9
108	Rapid fabrication of tin-copper anodes for lithium-ion battery applications. Journal of Alloys and Compounds, 2021, 867, 159031.	5.5	9

#	Article	IF	CITATIONS
109	Charge partitioning by intertwined metal-oxide nano-architectural networks for the photocatalytic dry reforming of methane. Chem Catalysis, 2022, 2, 321-329.	6.1	9
110	Effects of simultaneous displacive and ionizing radiations and of electric field on radiation damage in ionic crystals. Metallurgical and Materials Transactions A: Physical Metallurgy and Materials Science, 2004, 35, 2257-2266.	2.2	8
111	Direct observation of the Ni stabilising effect in interfacial (Cu,Ni)6Sn5 intermetallic compounds. Materialia, 2020, 9, 100530.	2.7	8
112	Sequential transmission electron microscopy observation of the shape change of gold nanorods under pulsed laser light irradiation. Microscopy (Oxford, England), 2019, 68, 174-180.	1.5	7
113	Significantly enhanced CO oxidation activity induced by a change in the CO adsorption site on Pd nanoparticles covered with metal–organic frameworks. Chemical Communications, 2020, 56, 3839-3842.	4.1	7
114	Catalytic Roles and Synergetic Effects of Iron-Group Elements on Monometals and Alloys for Electrochemical Oxidation of Ammonia. Bulletin of the Chemical Society of Japan, 2021, 94, 1292-1299.	3.2	7
115	Tuning 2D magnetism in Fe3+XGeTe2 films by element doping. National Science Review, 2022, 9, . Atomic locations of minor dopants and their roles in the stabilization of <mml:math< td=""><td>9.5</td><td>7</td></mml:math<>	9.5	7
116	xmlns:mml="http://www.w3.org/1998/Math/MathML"> <mml:mrow><mml:mi>i·</mml:mi><mml:mtext>â^'mathvariant="normal">C<mml:msub><mml:mi mathvariant="normal">u<mml:mn>6</mml:mn></mml:mi </mml:msub><mml:mi mathvariant="normal">S<mml:msub><mml:mi< td=""><td>2.4</td><td>nmi:mi 7</td></mml:mi<></mml:msub></mml:mi </mml:mtext></mml:mrow>	2.4	nmi:mi 7
117	mathvariant="normal">n <mml:mn>5</mml:mn> . Physi Nitrile hydrogenation to secondary amines under ambient conditions over palladium–platinum random alloy nanoparticles. Catalysis Science and Technology, 2022, 12, 4128-4137.	4.1	7
118	Hydrogen sorption behaviour of Mg-5wt.%La alloys after the initial hydrogen absorption process. International Journal of Hydrogen Energy, 2022, 47, 16132-16143.	7.1	7
119	Microstructure of CuAu-I-type ordered phase in III-V semiconductor alloys grown on a (001) substrate. Physical Review B, 1996, 54, 10814-10819.	3.2	6
120	Development of Novel Optical Fiber System for Cathodoluminescence Detection in High Voltage Transmission Electron Microscope. Materials Transactions, 2013, 54, 854-856.	1.2	6
121	The Electronic State of Hydrogen in the αâ€Phase of the Hydrogenâ€Storage Material PdH(D) _{<i>x</i>} : Does a Chemical Bond Between Palladium and Hydrogen Exist?. Angewandte Chemie, 2018, 130, 9971-9975.	2.0	6
122	Local structure investigations of accumulated damage in irradiated MgAl ₂ O ₄ . Journal of the American Ceramic Society, 2020, 103, 4654-4663.	3.8	6
123	<i>In Situ</i> TEM Investigation of Structural Changes in Ni Nanoparticle Catalysts under Gas Atmospheres: Implications for Catalyst Degradation. ACS Applied Nano Materials, 2021, 4, 2175-2182.	5.0	6
124	Interfacial reactions between Ga and Cu-xNi (x=0, 2, 6, 10, 14) substrates and the strength of Cu-xNi/Ga/Cu-xNi joints. Intermetallics, 2021, 133, 107168.	3.9	6
125	Subpercent Local Strains Due to the Shapes of Gold Nanorods Revealed by Data-Driven Analysis. ACS Nano, 2021, 15, 12077-12085.	14.6	6
126	Higher order Laue zone patterns in convergent beam electron diffraction and determinations of local lattice parameters in .ALPHA and .ALPHA.2-phases of a Cu-20at%Al alloy ISIJ International, 1989, 29, 191-197	1.4	6

#	Article	IF	CITATIONS
127	Quantitative Analysis of Ordered Structure in Multinary Alloys by the IKL-ALCHEMI Method and Its Application to Ordering Kinetics. Journal of Electron Microscopy, 1996, 45, 93-98.	0.9	5
128	Effects of Simultaneous Displacive and Ionizing Radiation in Ionic and Covalent Crystals. Defect and Diffusion Forum, 2002, 206-207, 53-74.	0.4	5
129	Atomistic observation of electron irradiation-induced defects in CeO ₂ . Materials Research Society Symposia Proceedings, 2013, 1514, 93-98.	0.1	5
130	Image contrast enhancement of Ni/YSZ anode during the sliceâ€andâ€view process in FIB‣EM. Journal of Microscopy, 2016, 261, 326-332.	1.8	5
131	A comparative characterization of defect structure in NiCo and NiFe equimolar solid solution alloys under in situ electron irradiation. Scripta Materialia, 2019, 166, 96-101.	5.2	5
132	Electrochemically enhanced Cu6Sn5 anodes with tailored crystal orientation and ordered atomic arrangements for lithium-ion battery applications. Acta Materialia, 2020, 201, 341-349.	7.9	5
133	Quantitative Characterization of the Thermally Driven Alloying State in Ternary Ir–Pd–Ru Nanoparticles. ACS Nano, 2022, 16, 1612-1624.	14.6	5
134	Compositional dependence of structures and hydrogen evolution reaction activity of platinum-group-metal quinary RuRhPdIrPt alloy nanoparticles. Chemical Communications, 2022, 58, 6421-6424.	4.1	5
135	Interpretation of High Resolution Transmission Electron Microscope Images of Short Range Ordered Ni ₄ Mo. Materials Transactions, JIM, 1998, 39, 914-919.	0.9	4
136	The atomic structure of disordered ion tracks in magnesium aluminate spinel. Jom, 2007, 59, 27-30.	1.9	4
137	Three-dimensional Visualization of Lattice Defects by Electron Tomography. Materia Japan, 2010, 49, 274-279.	0.1	4
138	Temperature dependent evolution of dislocation loops in YSZ under high energy electron irradiation. Transactions of the Materials Research Society of Japan, 2016, 41, 319-323.	0.2	4
139	Fabrication of Integrated Copperâ€Based Nanoparticles/Amorphous Metal–Organic Framework by a Facile Sprayâ€Drying Method: Highly Enhanced CO 2 Hydrogenation Activity for Methanol Synthesis. Angewandte Chemie, 2021, 133, 22457-22462.	2.0	4
140	Ni@onion-like carbon and Co@amorphous carbon: control of carbon structures by metal ion species in MOFs. Chemical Communications, 2021, 57, 5897-5900.	4.1	4
141	Phase Control of Solid-Solution Nanoparticles beyond the Phase Diagram for Enhanced Catalytic Properties. ACS Materials Au, 2022, 2, 110-116.	6.0	4
142	Time-Evolution of Long Range Ordering in CuAuPd Ternary Alloys. Materials Transactions, JIM, 1998, 39, 159-168.	0.9	3
143	Recent Development in Quantitative Electron Diffraction for Crystallography of Materials. Materials Transactions, JIM, 1998, 39, 927-937.	0.9	3
144	Three-Dimensional Imaging of a Long-Period Stacking Ordered Phase in Mg ₉₇ Zn ₁ Gd ₂ Using High-Voltage Electron Microscopy. Materials Transactions, 2016, 57, 918-921.	1.2	3

#	Article	IF	CITATIONS
145	Discovery of Hexagonal Structured Pd–B Nanocrystals. Angewandte Chemie, 2017, 129, 6678-6682.	2.0	3
146	Structural and Thermodynamic Studies of Hydrogen Absorption/Desorption Processes on PdPt Nanoparticles. Journal of Physical Chemistry C, 2019, 123, 9471-9478.	3.1	3
147	Coating of 2D Flexible Metal–Organic Frameworks on Metal Nanocrystals. Chemistry Letters, 2019, 48, 173-176.	1.3	3
148	Transition of Cationic Local Structures in Mg1-xNixAl2O4. Journal of Physical Chemistry C, 2021, 125, 5269-5277.	3.1	3
149	Enhanced Hydrogenation Catalytic Activity of Ruthenium Nanoparticles by Solidâ€Solution Alloying with Molybdenum. European Journal of Inorganic Chemistry, 2021, 2021, 1186-1189.	2.0	3
150	The Effects of Trace Sb and Zn Additions on Cu6Sn5 Lithium-Ion Battery Anodes. Journal of Nanoscience and Nanotechnology, 2020, 20, 5182-5191.	0.9	3
151	Atomic insights into the ordered solid solutions of Ni and Au in ÎCu6Sn5. Acta Materialia, 2022, 224, 117513.	7.9	3
152	In Situ Observation of Liquid Solder Alloys and Solid Substrate Reactions Using High-Voltage Transmission Electron Microscopy. Materials, 2022, 15, 510.	2.9	3
153	Co Nanoparticle Catalysts Encapsulated by BaO–La ₂ O ₃ Nanofractions for Efficient Ammonia Synthesis Under Mild Reaction Conditions. ACS Omega, 2022, 7, 24452-24460.	3.5	3
154	Kinetics of Ordered Domain Formation in Binary Alloys of D0 ₁₉ Type Order. Transactions of the Materials Research Society of Japan, 2015, 40, 325-329.	0.2	2
155	Statistical Evaluation of the Solid-Solution State in Ternary Nanoalloys. Journal of Physical Chemistry C, 2020, 124, 21843-21852.	3.1	2
156	Multi-scale 3D characterization of long period stacking ordered structure in Mg-Zn-Gd cast alloys. Microscopy (Oxford, England), 2014, 63, i25.2-i26.	1.5	1
157	Lattice Tetragonality and Local Strain Depending on Shape of Gold Nanoparticles. Microscopy and Microanalysis, 2019, 25, 2122-2123.	0.4	1
158	Frontispiece: A CO Adsorption Site Change Induced by Copper Substitution in a Ruthenium Catalyst for Enhanced CO Oxidation Activity. Angewandte Chemie - International Edition, 2019, 58, .	13.8	1
159	Cu–Pd–B Alloy Nanoparticles Synthesized by External Boron Doping Method. Chemistry Letters, 2021, 50, 611-614.	1.3	1
160	First Observation of Superconductivity in Molybdenum–Ruthenium–Carbon Alloy Nanoparticles. Chemistry Letters, 2021, 50, 596-598.	1.3	1
161	Effect of Spatial Correlation of Particles on Ostwald Ripening. , 1988, , 233-238.		1
162	Tomographic Dark-Field TEM Observation of Ordered Ni;Mo Variants. Materia Japan, 2007, 46, 792-792.	0.1	1

#	Article	IF	CITATIONS
163	Three-Dimensional Observation of Superlattice Domains in Ordering Alloys by DFTEM Tomography. Nihon Kessho Gakkaishi, 2008, 50, 314-319.	0.0	1
164	Atomistic Microstructures in Short-Range Ordered Alloys Nihon Kessho Gakkaishi, 2002, 44, 225-233.	0.0	1
165	Dynamics of Ordering with Phase Separation in Iron-Silicon Alloys. , 1988, , 315-320.		1
166	The Effect of Ru Precursor and Support on the Hydrogenation of Aromatic Aldehydes/Ketones to Alcohols. ChemCatChem, 2022, 14, .	3.7	1
167	Structural Disordering in Magnesium Aluminate Spinel Compounds under Ion-Beam Irradiation. Materials Research Society Symposia Proceedings, 2003, 792, 395.	0.1	Ο
168	Radiation Damage Effects in Insulators for Fusion Reactors: Microstructure Evolution in MgO-Al ₂ O ₃ System Oxide Crystals. Advances in Science and Technology, 2006, 45, 1961-1968.	0.2	0
169	Formation of Domain Structures in Ordering Processes of B2 and D03 Types. Materials Research Society Symposia Proceedings, 2006, 979, 1.	0.1	0
170	High Resolution Observation of MgAl ₂ O ₄ Irradiated with 350 MeV Au ions. Materia Japan, 2008, 47, 614-614.	0.1	0
171	Application of TDGL Model to B2 Type Ordering with Two Step Phase Separation in Fe-Ni-Al Alloys. Materials Research Society Symposia Proceedings, 2013, 1535, 5601.	0.1	Ο
172	Simulations of structure formation in B2 type ordering with two step phase separation in Fe-Ni-Al alloys. , 2013, , .		0
173	B22-P-06Ni/YSZ Interface in A Conventional Solid Oxide Fuel Cell. Microscopy (Oxford, England), 2015, 64, i105.2-i105.	1.5	0
174	B21-P-01STEM study of bimetallic Pd-Ru nanoparticles. Microscopy (Oxford, England), 2015, 64, i97.2-i97.	1.5	0
175	Reply to â€~Comments on "Evidence of the hydrogen release mechanism in bulk MgH2â€â€™. Scientific Reports, 2017, 7, 43720.	3.3	Ο
176	Recent Trend of Transmission Electron Microscopy and Application to Green Nano-technology. Journal of MMIJ, 2017, 133, 58-67.	0.3	0
177	PM-26Atomic insights into the Ni-stabilized hexagonal Î(Cu,Ni)6Sn5 intermetallic compound. Microscopy (Oxford, England), 2018, 67, i48-i48.	1.5	Ο
178	Frontispiz: A CO Adsorption Site Change Induced by Copper Substitution in a Ruthenium Catalyst for Enhanced CO Oxidation Activity. Angewandte Chemie, 2019, 131, .	2.0	0
179	In-Situ Observation of Liquid Solder Alloys and Solid Substrate Reactions Using High-Voltage Transmission Electron Microscopy. SSRN Electronic Journal, 0, , .	0.4	0
180	Defect Clusters in Yttria-stabilized Cubic-zirconia Irradiated with Ions and/or Electrons. Materia Japan, 2000, 39, 993-993.	0.1	0

#	Article	IF	CITATIONS
181	Radiation-Induced Defects in α-Alumina Irradiated with Ions under an Applied Electric Field. Materia Japan, 2003, 42, 906-906.	0.1	0
182	TEM-Tomography Observation of Ion-Irradiated FePt Nano-Granular Films. Materia Japan, 2004, 43, 1003-1003.	0.1	0
183	Electron Enrgy-Dependent Type of Dislocation Loops in CeO ₂ . Materia Japan, 2008, 47, 612-612.	0.1	0
184	Electron Tomography Observation of FePt Nanogranular Thin Films Irradiated with 210 MeV Xe Ions. Materia Japan, 2008, 47, 639-639.	0.1	0
185	In-situ Transmission Electron Microscopy Observation of Electron-beam-induced Defect-clusters in CaF ₂ Crystal. Materia Japan, 2008, 47, 647-647.	0.1	0
186	Element Mapping Around Grain Boundaries in Ca-doped β-Si ₃ N ₄ by Electron Spectroscopic Imaging. Materia Japan, 1998, 37, 981-981.	0.1	0
187	Observation of Dislocations in Thick Specimens Using by The High-Voltage Electron Microscopy with an Energy Filter. Materia Japan, 2016, 55, 597-597.	0.1	0
188	Atomic Displacements in Twinned Structures in a Gold Nanoparticle Irradiated with a Pulsed Laser Light. Materia Japan, 2016, 55, 583-583.	0.1	0
189	PM-11Lattice Strain Analysis in Gold Nanorods by Means of Atomic Resolution HAADF-STEM Experiments and Molecular Dynamics Simulations. Microscopy (Oxford, England), 2017, 66, i23-i23.	1.5	0
190	Kyushu University Ultramicroscopy Platform for Nanomaterial Developing. Materia Japan, 2019, 58, 746-753.	0.1	0